JMEPEG
https://doi.org/10.1007/s11665-024-09580-7

1059-9495/$19.00

ORIGINAL RESEARCH ARTICLE

Influence of Annealing Heat Treatment on the Microstructure and Mechanical Properties of Multilayer 316L-TiC Composite Fabricated by Selective Laser Melting

Sasan Yazdani, Süleyman Tekeli, Tolga Yilmaz, and Mükerrem Nur Adanir

Submitted: 7 February 2024 / Revised: 27 March 2024 / Accepted: 5 April 2024

Selective laser melting (SLM) can induce residual stresses in components, especially those with multilayer structures and varying thermal properties. This study investigates the effect of annealing post-heat treatment on the microstructure and mechanical properties of multilayer 316L stainless steel composite reinforced with TiC particles. Three-layer composite samples of 316L/316L-5%TiC/316L-10%TiC (wt.%) were fabricated using the SLM method. One set of samples was then annealed at 1100 °C for 1 h followed by air cooling, while another set remained as-produced. Both sets were characterized using optical and electron microscopy. Additionally, the wear behavior and the hardness of samples were evaluated. Results reveal defect-free interfaces and increased hardness in TiC-reinforced layers after annealing, along with improved ductility. The microstructure, initially with fusion lines and elongated austenite grains, transitioned to an equiaxed grain microstructure after annealing, with no observable cellular structure. Annealing enhanced both the ductiliy of the pure 316L layer and the overall strength of the multilayer sample. Despite a slight decrease in wear performance after annealing treatment, the TiC reinforcement effectively improved wear performance for the layers. This study highlights the importance of annealing in optimizing the microstructure and mechanical performance of SLM-produced functionally graded composites for advanced applications.

Keywords annealing post-heat treatment, multilayer 316L-TiC composite, selective laser melting, wear

1. Introduction

The widespread adoption of selective laser melting (SLM) additive manufacturing (AM) in various industries has opened new frontiers in the production of advanced materials and composites (Ref 1-8). Innovative applications include the development of functionally graded materials (FGM), where properties are systematically graded by adjusting the chemical composition to meet specific requirements (Ref 9-14). This enables the precise adjustment of mechanical properties, such as hardness and wear resistance, as well as other characteristics like resistance to high temperatures. SLM plays a crucial role in the production of FGMs, a capability not achievable with conventional manufacturing methods.

Sasan Yazdani, Faculty of Materials Engineering, Sahand University of Technology, Tabriz, Iran; and Department of Metallurgy and Materials Engineering, Faculty of Technology, Gazi University, 06560 Ankara, Turkey; and **Süleyman Tekeli, Tolga Yilmaz,** and **Mükerrem Nur Adanir**, Department of Metallurgy and Materials Engineering, Faculty of Technology, Gazi University, 06560 Ankara, Turkey. Contact e-mails: yazdani@sut.ac.ir and sasan.yazdani@gazi.edu.tr.

One example is the use of SLM to produce functionally graded materials consisting of 316L stainless steel (SS) and TiC ceramic particles. TiC, known for its hardness and stability at elevated temperatures, serves as a valuable complement to metal matrices. 316L SS, widely employed in various applications owing to its excellent corrosion resistance and formability, nevertheless faces challenges related to low strength and wear performance (Ref 15, 16).

The addition of ceramic particles, such as TiC, has been shown to be effective in producing wear-resistant composites (Ref 17-23). However, when reinforcing with ceramic particles, there is a trade-off between hardness and wear resistance on the one hand and ductility and toughness on the other hand. By grading the TiC volume fraction in the matrix using SLM, both the hardness and toughness of TiC and the ductility of the 316L SS matrix can be utilized.

In processes characterized by rapid cooling rates and significant thermal gradients, there is a risk of residual stresses in the components (Ref 24). This problem is even more pronounced in the SLM process, where the cooling rates remain very high despite the implementation of various scanning strategies to mitigate them (Ref 25-30). As a solution, the application of post-heat treatment annealing has been proposed to relive stress and improve mechanical properties (Ref 31-36).

While post-heat treatment annealing has been employed to relieve residual stresses in SLM-fabricated components, there is a notable absence of reports on its impact on multilayer composites produced by this method. The objective of this research is to investigate the influence of annealing heat

Published online: 10 June 2024

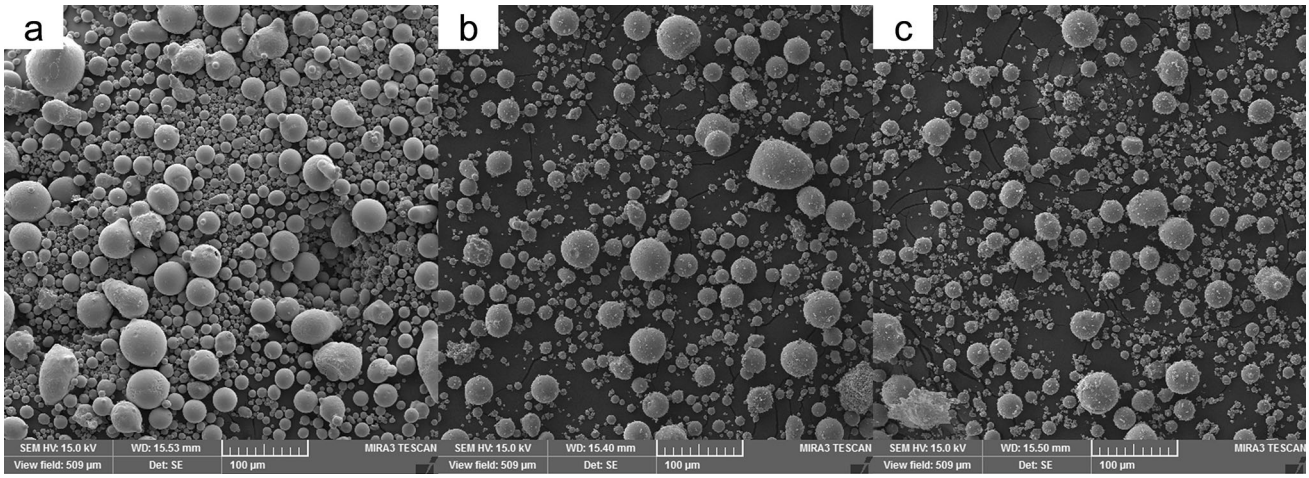

Fig. 1 Scanning electron microscopy images of the powders: (a) 316L SS, (b) 316L SS mixed with 5 wt.% TiC, and (c) 316L SS mixed with 10 wt.% TiC

treatment on the microstructure and mechanical properties of the multilayer 316L-TiC composite fabricated by the SLM process.

2. Experimental Procedure

2.1 Material

The raw materials utilized in this study included AISI 316L SS powder featuring particle sizes ranging from 15 to 50 μm and titanium carbide (TiC) powder with particles measuring less than 20 μm. The specifications of these powders adhered to the requirements of the SLM powder feeding system.

To achieve two distinct powder concentrations, namely, 316L-5TiC and 316L-10TiC (wt.%), a thorough mixing process was carried out using a turbo mixer for 4 h. This step involved meticulous blending of 316L and TiC powders. Figure 1(a), (b), and (c) displays scanning electron microscopy images of plane 316L and composite layers, respectively. As observed, the 316L and TiC particles are well mixed, with some submicron TiC particles adhering to the 316L particles, ensuring a homogeneous distribution of TiC in the 316L matrix after the SLM process. Before initiating the SLM process, the blended powders underwent a drying phase in an oven set at a temperature of 103 °C, lasting for 1 h. This meticulous preparation ensured the optimal condition of the powder feedstock for subsequent processing.

2.2 Selective Laser Melting Process

A laboratory SLM system was used to produce multilayer samples consisting of three layers of 316L SS, 316L SS-5TiC, and 316L SS-10TiC (wt.%). The SLM process began with data preparation using CAD software and ended with the removal of the manufactured samples from the substrate. To protect against oxidation, the samples were produced in a controlled oxygen atmosphere using argon inert gas. Prior to production, the chamber was evacuated and filled with argon to reduce the oxygen content to a specific level.

In this study, the parallel line scan strategy was applied, which is widely accepted in SLM due to its easy programming and wide applicability. To avoid distortions and deformations in the resulting samples, a rotation angle of 67° in the laser direction was implemented for each successive layer during sample fabrication (Ref 37). This specific rotation angle ensures that the laser beam direction is not repeated over a significant number of layers (several thousand), thus minimizing residual stresses in the finished part. Figure 2 illustrates the scanning strategy used in this study.

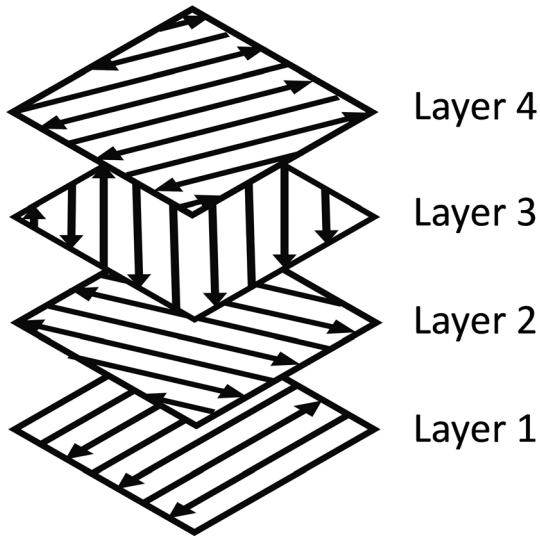

Fig. 2 The parallel line scanning strategy employed in the current study, features a 67° rotation at each new layer scanned

2.3 Heat Treatment

Heat treatment was performed in a tube furnace by austenitizing at 1100 °C for 1 h, followed by cooling in air to room temperature under an argon gas atmosphere. At this temperature, the solubility of TiC in the matrix is almost negligible (Ref 38), and only phase transformations occur within the matrix.

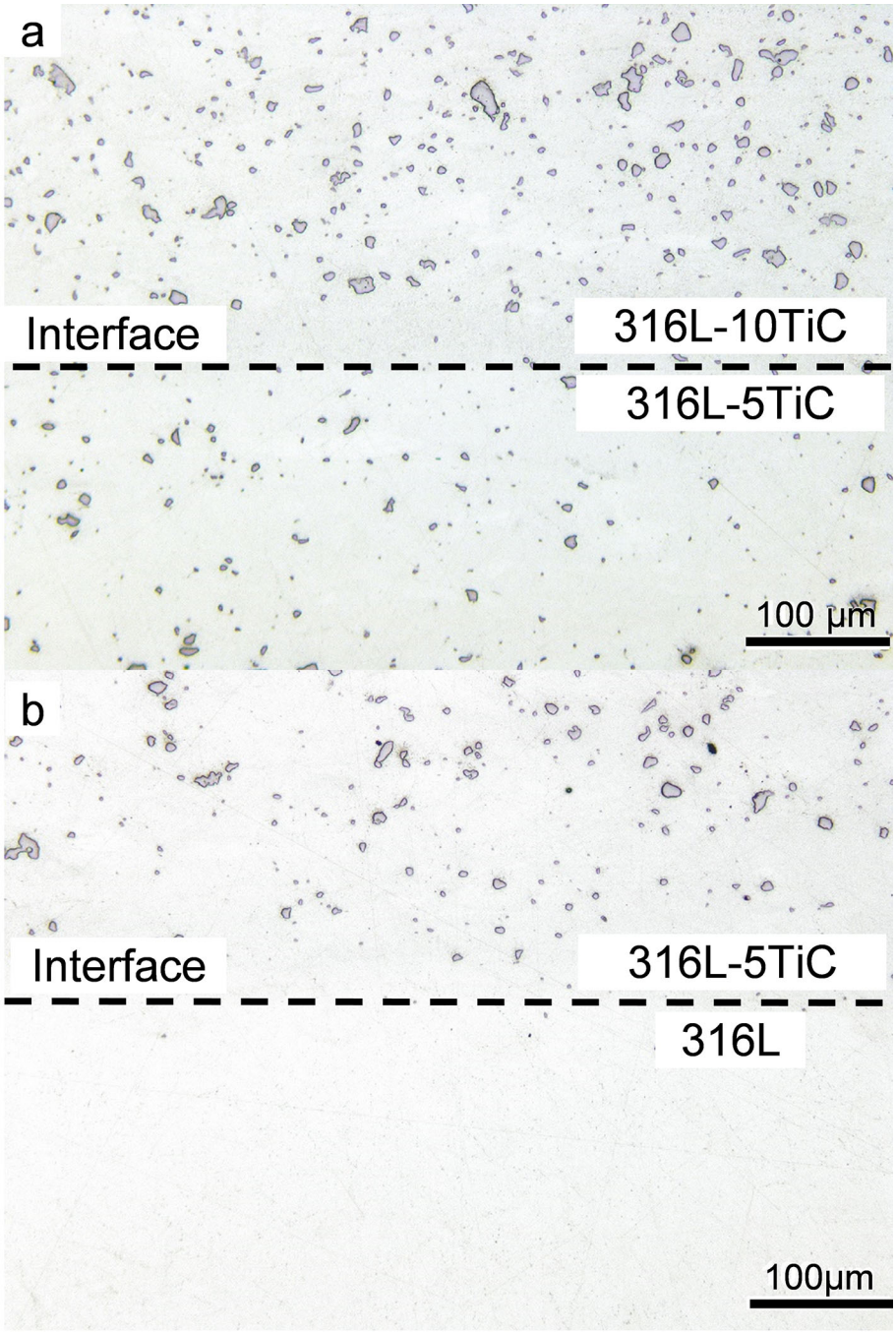

Fig. 3 Images of fabricated composite layers in their as-polished condition: (a) 316L-5TiC/316L-10TiC and (b) 316L/316L-5TiC. Dashed lines indicate the interface location between the layers.

2.4 Microstructural Observations

The fabricated specimens were subjected to extensive microstructural analysis employing conventional metallographic methods. Grinding was performed using silicon carbide abrasive papers with grit sizes ranging from 60 to 3000, followed by automated polishing using diamond paste with particle sizes of 1 and 0.25 μm. The specimens were then subjected to etching with Glyceregia reagent for the duration of 60-120 s to reveal the microstructural features. The examination and characterization of these features, along with a detailed analysis, was facilitated by a Leica DFC 450 microscope. SEM observations were performed using a Jeol JEM 6060 LV scanning electron microscope, with the operating voltage set between 5 and 15 kV. To maintain sufficient focus and image clarity, a working distance of 10 mm was maintained throughout the observations.

2.5 Mechanical Property Evaluations

The Vickers hardness of the layers was measured using a Qness Q30M hardness tester instrument at room temperature. Prior to testing, the surface of the sample was carefully prepared, and the indentations were made with a force of 9.8 N including a 10-s relaxation pause. Multiple indentations were made on each layer surface, and the average was reported.

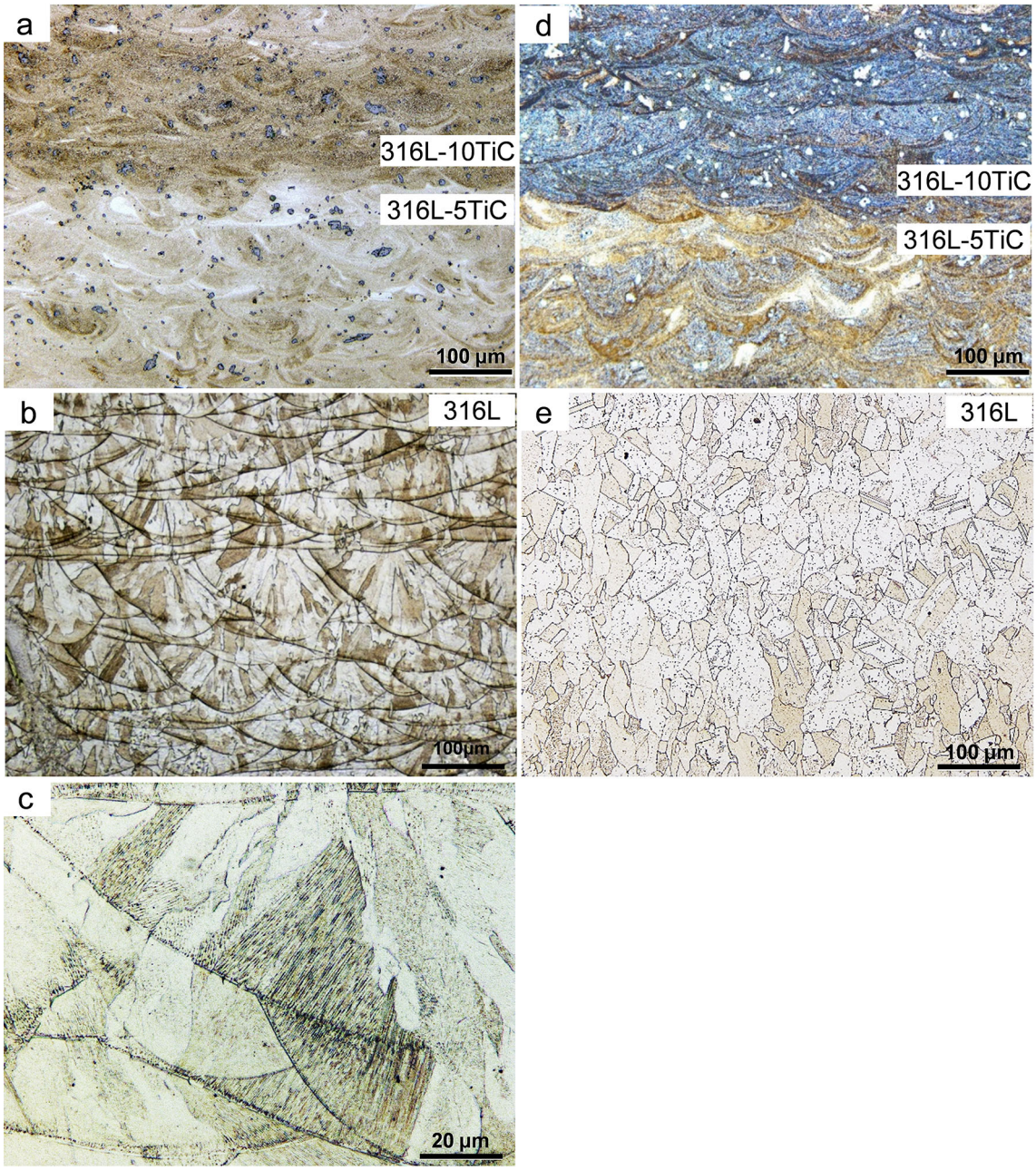

Fig. 4 Images of the fabricated layers after etching with Glyceregia reagent for (a) 316L-5TiC/316L-10TiC, (b) and (c) 316L layers before annealing, and (d) 316L-5TiC/316L-10TiC, and (e) 316L layers after annealing post-treatment. The plane surfaces of images are parallel to build direction.

Tensile test was performed on samples prepared from the layers of the produced composite in accordance with the JIS Z 2201 standard (Ref 39) at room temperature using an Instron 3369 universal testing machine with the crosshead speed set at 1 mm/min. Load and displacement data were recorded to characterize the stress–strain behavior of the specimens.

The wear test was performed at room temperature using a T10/20 TURQUDSE 2.0 ball on disk Tribometer. The test was performed at a speed of 0.1 m/s and a constant load of 15 N, with a specified wear distance of 500 m. In this test configuration, the specimens were disk shaped, while Al_2O_3 ceramic balls acted as the abrasive. The test procedure was based on the ASTM G 133-95 standard, and the wear behavior and the resulting wear tracks were analyzed and evaluated based on the wear tracks and the observed wear mechanisms. In addition, surface topography measurements were made on the worn samples using a Huvitz/HRM-300 Optic Profilometer.

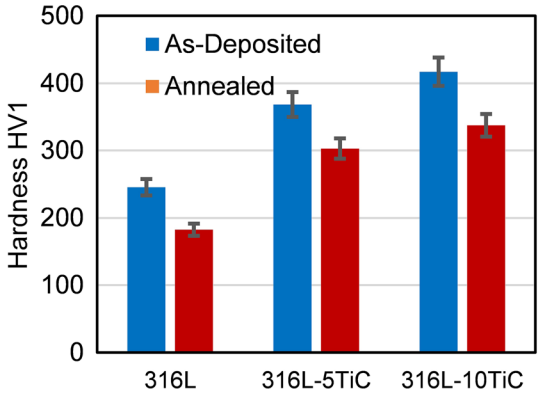

Fig. 5 Hardness of 316L, 316L-5TiC, and 316L-10TiC layers in as-deposited and annealed conditions.

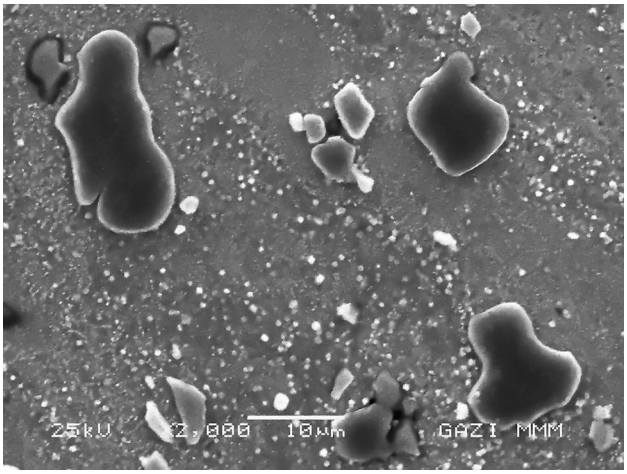

Fig. 6 SEM micrograph from the 316L-10TiC layer indicating the distribution of submicron-sized TiC particles along the larger particles

3. Results and Discussion

3.1 Microstructure

Figure 3(a) and (b) shows optical micrographs of the as-polished 316L and 316L-TiC composite layers. Notably, the images show the absence of microporosities, indicating a dense and well-compacted microstructure. Furthermore, the TiC particles exhibit a highly homogeneous distribution throughout the composite layer, with no observable evidence of clustering or agglomeration. This uniform dispersion suggests effective incorporation of the ceramic phase, which could positively affect the mechanical properties of the material. Additionally, the interfaces at 316L/316L-5TiC and 316l-5TiC/316L-10TiC composite layers appear defect-free, exhibiting excellent continuity and adhesion between the distinct regions. This intimate interfacial contact is crucial for optimal load transfer and overall composite performance.

Figure 4(a), (b), (c), (d), and (e) presents the micrographs of the 316L-105TiC, 316L-5TiC, and 316L layers, respectively, after etching with Glyceregia reagent before and after annealing post-heat treatment. Figure 4(b) shows the intricate details within the 316L layer. The melt lines are clearly visible, revealing the formation of melt pools created by the passage of the laser during the AM process. It is noteworthy that the average width of these melt pools, as seen in the image, exceeds the selected hatch spacing of 60 μm. This phenomenon is due to the inherent misalignment between the metallurgical surface and the laser direction with each new layer, a consequence of the rotation of the laser during subsequent layers.

Figure 4(b) also reveals that grains extended beyond individual melt pools into subsequent layers, with some grains extending over several layers, indicating that certain austenite grains from the preceding layers were partially melted, followed by epitaxial grain growth on these partially melted grains. This observation is consistent with the epitaxial growth mode reported by other researchers (Ref 40, 41). Furthermore, the microscope image illustrates the directional growth of the grains from bottom to top, which is opposite to the direction of heat transfer. This indicates the interplay between thermal gradients and grain growth mechanisms during the AM process. It is worth noting that the grains are not visible in the TiC-containing layers (Fig. 4a) due to the influence of TiC particles that refine the grain structure.

Figure 4(c) presents a magnified image of the 316L microstructure, revealing a characteristic cellular structure within the randomly oriented grains. This cellular morphology is a direct result of the exceptionally high cooling rates, typically ranging from 10^3 to 10^4 °C/s (Ref 42) during the SLM process. These rapid cooling rates, which are achieved due to the small melt pool size and the high laser travel speed, have a significant impact on the solidification process. At such intense cooling rates, the solidification process is so rapid that the formation of secondary dendrite arms is severely limited. This limitation contrasts with slower cooling scenarios where secondary arms readily develop, and eventually form a dendritic structure. Rapid heat removal promotes the formation of cellular interfaces along the solidification fronts. Stainless steel structures produced by SLM typically display three times the strength and improved mechanical properties of those produced by conventional methods. This improvement can be attributed to a refined cellular structure and higher dislocation density (Ref 43).

Figure 4(d) and (e) presents the annealed images of the fabricated layers after etching with Glyceregia. In Fig. 4(d), the austenite grain boundaries are not visible, similar to Fig. 4(a). In Fig. 4(e), the microstructure of the 316L layer reveals grown austenite grains, some of which showing annealing twinning. Very fine precipitates are observed in the microstructure after annealing treatment. Transmission electron microscopy studies conducted by Salman et al. (Ref 44) on the annealed microstructure of 316L produced by SLM revealed an amorphous structure for the precipitates, which are rich in Mn and Si. The cellular structure observed in the non-heat treated sample is not evident in the annealed sample. The studies indicated that cellular walls are composed of dislocation tangles accompanied by segregation of Mn, Mo, and Cr elements. Therefore, the disappearance of the cellular structure can be attributed to the reduction in dislocation density during annealing. The average grain size was measured to be 25 $\pm$ 7 μm in the annealed sample.

3.2 Mechanical Properties

Figure 5 displays the Vickers hardness (HV1) of fabricated layers, both in the as-built and annealed conditions. The hardness of each layer reflects an average of at least five

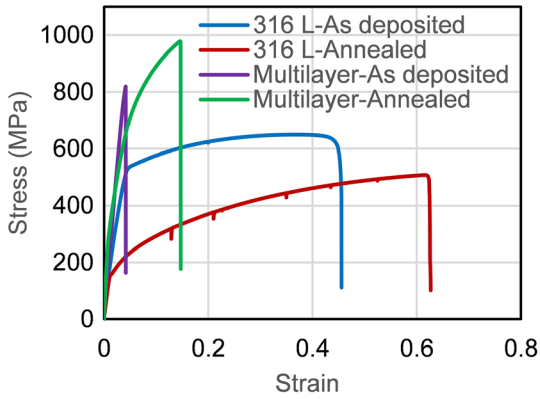

Fig. 7 Stress–strain curves for 316L and multilayer samples in as-deposited and annealed conditions

Table 1 Ultimate tensile strength (UTS), yield strength (YS), and elongation of 316L and multilayer SLM samples before and after annealing post-heat treatment

Sample	UTS, MPa	YS, MPa	El, %
316L	645 ± 10	530 ± 7	45 ± 3
316L-annealed	508 ± 10	170 ± 5	62 ± 2
Multilayer	820 ± 10	…	7 ± 1
Multilayer-annealed	979 ± 10	290 ± 5	17 ± 1

measurements. The figure clearly shows a significant increase in the hardness of 316L layer when reinforced with TiC particles. In particular, the hardness values for 316L, 316L-5TiC, and 316L-10TiC layers are 245, 368, and 417 HV1, respectively. The fine cellular structure and high dislocation density within the austenite matrix contribute significantly to the hardness and strength of the material (Ref 45). These properties result from the rapid cooling rates inherent to the SLM process. The presence of TiC particles further enhances hardness through two mechanisms: particle strengthening and microstructural refinement. The hard TiC particles impede dislocation movement, preventing plastic deformation and increasing hardness. The submicron TiC particles refine the surrounding matrix, creating more grain boundaries that also imped dislocation movement (Ref 46). Figure 6 shows the scanning electron microscopy image of the 316L-10TiC matrix, where both submicron and larger TiC particles can be observed. AlMangour et al. (Ref 17) suggest that the formation of α/martensite during SLM may also contribute to increased hardness.

Annealing resulted in a decrease in hardness of approximately 60-70 Vickers across all layers due to two primary microstructural factors: coarsening and dislocation recovery. Annealing promoted grain growth, coarsening the microstructure and reducing the number of grain boundaries, which act as barriers to dislocation movement and contribute to hardness. On the other hand, it facilitated dislocation recovery, reducing the overall density and consequently lowering the resistance to plastic deformation.

Despite the softening effect of annealing, layers containing TiC particles retain higher hardness compared to the unreinforced 316L layer. This is because the presence of TiC particles mitigates the softening mechanisms associated with annealing, while maintaining their strengthening influence through particle reinforcement.

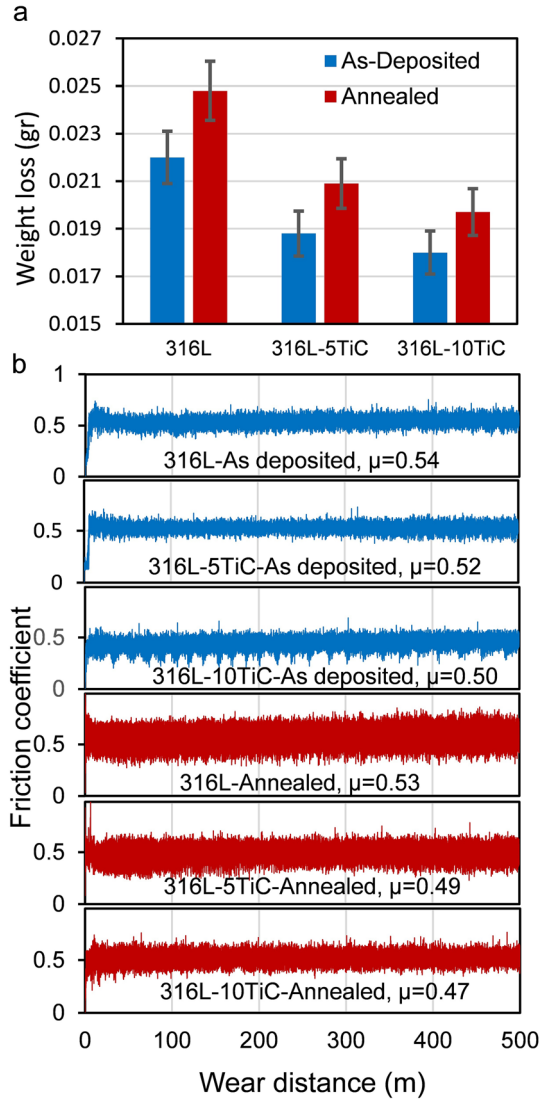

Fig. 8 (a) Weight loss of 316L, 316L-5TiC, and 316L-10TiC layers in as-deposited and annealed conditions after wear test and (b) the corresponding friction coefficients

Figure 7 presents the stress–strain curves of both single and multilayer 316L samples, with corresponding test results listed in Table 1. These results are presented for both the as-deposited and annealed post-treatment conditions. Samples were prepared parallel to the substrate for consistency. The 316L layer exhibits an impressive elongation of 45%, as shown in the figure. This exceptional ductility implies minimal microporosity or other defects that could negatively affect its formability. Notably, these properties exceed the minimum requirements of the ASTM A240 standard and even exceed data reported in the literature for 316L produced by SLM (Ref 47). In contrast, the multilayer sample with layers oriented parallel to the longitudinal direction exhibited brittle fracture behavior, as shown in Fig. 7. This brittleness is due to the high volume fraction of brittle TiC particles combined with the reinforced metal matrix within the composite layers, effectively eliminating any ductility. However, the annealing process successfully introduced some ductility, resulting in increased strength prior to the final fracture. Figure 7 further highlights the increased ductility observed in the 316L layer following the annealing post-

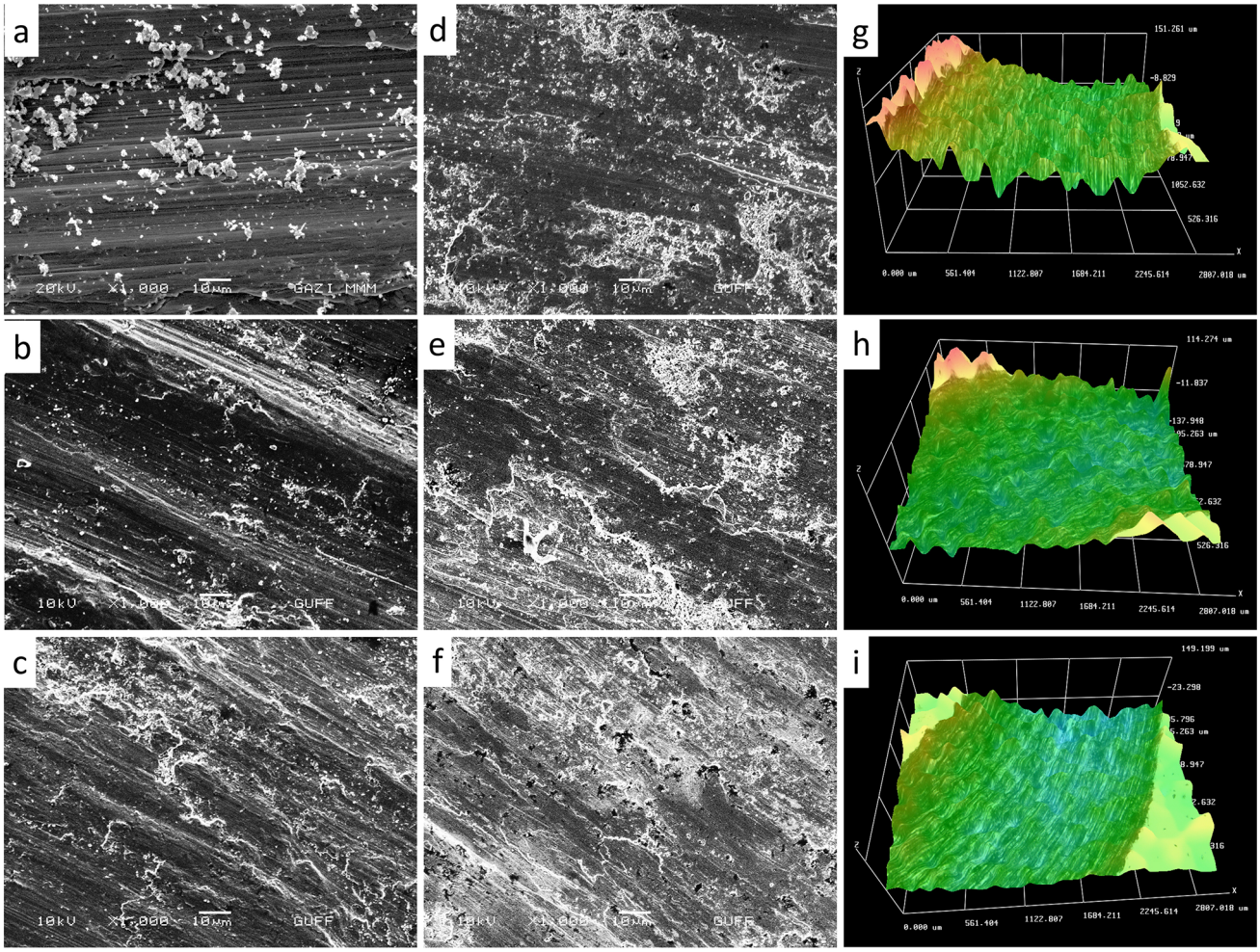

Fig. 9 Scanning electron microscope images of wear tracks for (a) 316L, (b) 316L-5TiC, and (c) 316L-10TiC layers in as-deposited condition and (d)-(f) in annealed conditions, respectively. (g)-(i) Surface topography of the wear tracks corresponding to 316L, 316L-5TiC, and 316L-10TiC layers in annealed condition, respectively

treatment. This improvement can be attributed to the relaxation of residual stresses and the recovery of the dislocation microstructure, both of which contribute to improved material flexibility.

Figure 8 presents the weight loss of the fabricated layers in as-deposited and annealed post-heat treatment conditions, along with the corresponding friction coefficient profiles. The weight loss decreases from the 316L layer to the composite layers containing 5 and 10% TiC, respectively. In addition, the weight loss is higher for the layers after the annealing post-heat treatment. A similar trend is observed for the friction coefficient.

Friction coefficient profiles can be divided into two regions: running-in and steady state, under dry wear conditions (Ref 48, 49). The initial surface roughness determines the running-in time until the steady state is reached. Based on the friction coefficient profiles in Fig. 8, the running-in distance is very short, and there is not much difference among samples, considering that they were polished before the test and had a smooth surface. After this stage, the wear reaches the steady-state stage. The friction coefficient values shown in the figure are the average of the profile for the entire wear distance. Higher friction coefficient values correspond to more severe contact between surfaces, which consequently increases stress and weight loss. Several factors such as the amount of load, number of cycles or wear distance, and area of contact influence the wear behavior of the material. In the samples of this study, these parameters were identical. However, the hardness of the matrix and the amount of TiC ceramic particles were different among samples. The annealing post-heat treatment also influenced the residual stresses, which could influence the wear performance. The higher the initial hardness, the better the wear performance. This explains the lower weight loss of TiC-containing layers and, in contrast, the higher weight loss for annealed samples. The annealing treatment generally increased the weight loss in all layers, although the effect was less pronounced in TiC-containing layers. This suggests that while annealing may slightly soften the matrix, the presence of TiC particles still provides superior wear resistance compared to the unreinforced 316L layer even after heat treatment.

Figure 9 (a), (b), (c), (d), (e), and (f) reveals the wear tracks of 316L, 316L-5TiC, and 316L-10TiC layers in both as-deposited and annealed states. The presence of debris on the worn surfaces, confirmed by EDS analysis to be oxygen-rich oxidized particles, suggests material removal during wear. Notably, these particles are more abundant in the 316L layer, indicating greater material loss due to its lower hardness without TiC reinforcement. Furthermore, deeper scars are evident in the 316L wear track compared to the TiC-reinforced

counterparts. This observation directly points to the effectiveness of TiC particles in mitigating wear damage and promoting smoother surfaces. Based on these images, abrasive wear appears to be the dominant mechanism, with a higher intensity in the 316L layer. The results shown in Fig. 9 are consistent with the visual observations and show a significant reduction in weight loss with increasing TiC content. The worn surfaces of the annealed layers were analyzed using optical profilometer images, as shown in Fig. 9(g), (h), and (i) for the 316L, 316L-5TiC, and 316L-10TiC layers, respectively. These images provide further insight into the surface topography and are consistent with the observed wear patterns and loss of each layer.

4. Conclusions

Investigation of the influence of annealing heat treatment on the microstructure and mechanical properties of 316L-TiC multilayer composite produced by selective laser melting leads to the following conclusions:

- The interface between 316L stainless steel and TiC-containing layers was found to be defect-free.
- The TiC-reinforced layers exhibit significantly increased hardness compared to the unreinforced 316L layer, even after annealing. This underscores the robustness of TiC particle reinforcement in maintaining material strength and durability.
- The remarkable ductility of the 316L layer observed in tensile tests exceeded ASTM standards and published data in the literature. The multilayer sample exhibited brittle behavior. However, annealing improved ductility and strength due to stress relaxation and microstructure recovery.
- The TiC reinforcement effectively improved the wear performance of the layers. The observed decrease in weight loss with increasing TiC content, despite the influence of annealing treatments, highlights the superior wear resistance provided by TiC reinforcement.

Acknowledgments

The authors would like to thank the Scientific and Technological Research Council of Turkey (TÜBİTAK), for the support through the 2221 Fellowship Program for Visiting Scientists and Scientists on Sabbatical Leave. SY expresses his gratitude to Sahand University of Technology for granting sabbatical leave to facilitate the completion of this research.

Competing interest

The authors declare that they have no known competing financial interests or personal relationships that could appear to have influence the work reported in this paper.

References

1. I. Fidan, O. Huseynov, M.A. Ali, S. Alkunte, M. Rajeshirke, A. Gupta, S. Hasanov, K. Tantawi, E. Yasa, and O. Yilmaz, Recent Inventions in Additive Manufacturing: Holistic Review, *Inventions*, 2023, **8**(4), p 103. https://doi.org/10.3390/inventions8040103
2. F. Venturi and R. Taylor, Additive Manufacturing in the Context of Repeatability and Reliability, *J. Mater. Eng. Perform.*, 2023, **32**(15), p 6589–6609. https://doi.org/10.1007/s11665-023-07897-3
3. A. Das, V. Yadav, B. AlMangour, H.C. Prasad, N. Sathish, M. Ashiq, and A.K. Srivastava, Additive Manufacturing of Graphene Reinforced 316L Stainless Steel Composites with Tailored Microstructure and Mechanical Properties, *Mater. Chem. Phys.*, 2023, **303**, p 127826. https://doi.org/10.1016/j.matchemphys.2023.127826
4. A. Mandal, J.K. Tiwari, B. AlMangour, A. Das, N. Sathish, R.K. Sharma, P. Rajput, and A.K. Srivastava, Microstructural and Thermal Expansion Behaviour of Graphene Reinforced 316L Stainless Steel Matrix Composite Prepared via Powder Bed Fusion Additive Manufacturing, *Results Mater.*, 2021, **11**, p 100200. https://doi.org/10.1016/j.rinma.2021.100200
5. T. Larimian, M. Kannan, D. Grzesiak, B. AlMangour, and T. Borkar, Effect of Energy Density and Scanning Strategy on Densification, Microstructure and Mechanical Properties of 316L Stainless Steel Processed via Selective Laser Melting, *Mater. Sci. Eng. A*, 2020, **770**, p 138455. https://doi.org/10.1016/j.msea.2019.138455
6. B. AlMangour, Y.-K. Kim, D. Grzesiak, and K.-A. Lee, Novel TiB2-Reinforced 316L Stainless Steel Nanocomposites with Excellent Room- and High-Temperature Yield Strength Developed by Additive Manufacturing, *Compos. B Eng.*, 2019, **156**, p 51–63. https://doi.org/10.1016/j.compositesb.2018.07.050
7. B. AlMangour, D. Grzesiak, T. Borkar, and J.-M. Yang, Densification Behavior, Microstructural Evolution, and Mechanical Properties of TiC/316L Stainless Steel Nanocomposites Fabricated by Selective Laser Melting, *Mater. Des.*, 2018, **138**, p 119–128. https://doi.org/10.1016/j.matdes.2017.10.039
8. B. AlMangour, D. Grzesiak, and J.-M. Yang, Rapid Fabrication of Bulk-Form TiB2/316L Stainless Steel Nanocomposites with Novel Reinforcement Architecture and Improved Performance by Selective Laser Melting, *J. Alloys Compd.*, 2016, **680**, p 480–493. https://doi.org/10.1016/j.jallcom.2016.04.156
9. L. Yan, Y. Chen, and F. Liou, Additive Manufacturing of Functionally Graded Metallic Materials using Laser Metal Deposition, *Addit. Manuf.*, 2020, **31**, p 100901. https://doi.org/10.1016/j.addma.2019.100901
10. Y. Li, Z. Feng, L. Hao, L. Huang, C. Xin, Y. Wang, E. Bilotti, K. Essa, H. Zhang, and Z. Li, A Review on Functionally Graded Materials and Structures via Additive Manufacturing: From Multi-scale Design to Versatile Functional Properties, *Adv. Mater. Technol.*, 2020, **5**(6), p 1900981. https://doi.org/10.1002/admt.201900981
11. M. Ostolaza, J.I. Arrizubieta, A. Lamikiz, S. Plaza, and N. Ortega, Latest Developments to Manufacture Metal Matrix Composites and Functionally Graded Materials Through AM: A State-of-the-Art Review, *Materials*, 2023, **16**(4), p 1746. https://doi.org/10.3390/ma16041746
12. R. Nandhakumar and K. Venkatesan, A Process Parameters Review on Selective Laser Melting-Based Additive Manufacturing of Single and Multi-Material: Microstructure, Properties, and Machinability Aspects, *Mater. Today Commun.*, 2023 https://doi.org/10.1016/j.mtcomm.2023.105538
13. S.A. Tyagi and M. Manjaiah, Laser Additive Manufacturing of Titanium-Based Functionally Graded Materials: A Review, *J. Mater. Eng. Perform.*, 2022, **31**(8), p 6131–6148. https://doi.org/10.1007/s11665-022-07149-w
14. P. Kumar, K.K. Sadasivuni, B. Al Mangour, and M.S.A. Bin Majid, *High-Performance Composite Structures*, Springer, Berlin, 2022
15. H.T. Serindağ and G. Çam, Characterizations of Microstructure and Properties of Dissimilar AISI 316L/9Ni Low-Alloy Cryogenic Steel Joints Fabricated by Gas Tungsten Arc Welding, *J. Mater. Eng. Perform.*, 2023, **32**(15), p 7039–7049. https://doi.org/10.1007/s11665-022-07601-x
16. A.V. Radhamani, H.C. Lau, A.V. Krishnan, M. Kamaraj, and S. Ramakrishna, AISI 316L Stainless Steel Tribological Behavior under Sliding and Erosive Conditions: A Comparison between Spark Plasma Sintering, Laser Metal Deposition, and Cold Spraying, *J. Mater. Eng. Perform.*, 2023 https://doi.org/10.1007/s11665-023-08548-3
17. B. AlMangour, D. Grzesiak, and M. Jenn, Selective Laser Melting of TiC Reinforced 316L Stainless Steel Matrix Nanocomposites: Influence of Starting TiC Particle Size and Volume Content, *Mater. Des.*, 2016, **104**, p 141–151. https://doi.org/10.1016/j.matdes.2016.05.018

18. Z. Zhao, J. Li, P. Bai, H. Qu, M. Liang, H. Liao, L. Wu, P. Huo, H. Liu, and J. Zhang, Microstructure and Mechanical Properties of TiC-Reinforced 316L Stainless Steel Composites Fabricated using Selective Laser Melting, *Metals*, 2019, **9**(2), p 267. https://doi.org/10.3390/met9020267
19. S. Zhao, X. Shen, J. Yang, W. Teng, and Y. Wang, Densification Behavior and Mechanical Properties of Nanocrystalline TiC Reinforced 316L Stainless Steel Composite Parts Fabricated by Selective Laser Melting, *Opt. Laser Technol.*, 2018, **103**, p 239–250. https://doi.org/10.1016/j.optlastec.2018.01.005
20. B. AlMangour, M.-S. Baek, D. Grzesiak, and K.-A. Lee, Strengthening of Stainless Steel by Titanium Carbide Addition and Grain Refinement during Selective Laser Melting, *Mater. Sci. Eng. A*, 2018, **712**, p 812–818. https://doi.org/10.1016/j.msea.2017.11.126
21. B. AlMangour, D. Grzesiak, J. Cheng, and Y. Ertas, Thermal Behavior of the Molten Pool, Microstructural Evolution, and Tribological Performance during Selective Laser Melting of TiC/316L Stainless Steel Nanocomposites: Experimental and Simulation Methods, *J. Mater. Process. Technol.*, 2018, **257**, p 288–301. https://doi.org/10.1016/j.jmatprotec.2018.01.028
22. W. Zhai, Z. Zhu, W. Zhou, S.M.L. Nai, and J. Wei, Selective Laser Melting of Dispersed TiC Particles Strengthened 316L Stainless Steel, *Compos. B Eng.*, 2020, **199**, p 108291. https://doi.org/10.1016/j.compositesb.2020.108291
23. A. Bhowmik, W. Zhai, W. Zhou, and S.M.L. Nai, Characterization of Carbide Particle-Reinforced 316L Stainless Steel Fabricated by Selective Laser Melting, *Mater Charact*, 2021, **179**, p 111360. https://doi.org/10.1016/j.matchar.2021.111360
24. F. Chen, W. Guo, J. Li, Y. Liu, C. Zhang, J. Lu, Z. Huang, and Q. Shen, Residual Stress Control of TiC-Enhanced NiTi Shape Memory Alloys Fabricated by Laser Engineered Net Shaping, *J. Mater. Eng. Perform.*, 2023 https://doi.org/10.1007/s11665-023-09054-2
25. L. Mugwagwa, D. Dimitrov, S. Matope, and I. Yadroitsev, Evaluation of the Impact of Scanning Strategies on Residual Stresses in Selective Laser Melting, *Int. J. Adv. Manuf. Technol.*, 2019, **102**, p 2441–2450. https://doi.org/10.1007/s00170-019-03396-9
26. Z. Xiao, C. Chen, H. Zhu, Z. Hu, B. Nagarajan, L. Guo, and X. Zeng, Study of Residual Stress in Selective Laser Melting of Ti6Al4V, *Mater. Des.*, 2020, **193**, p 108846. https://doi.org/10.1016/j.matdes.2020.108846
27. Z.-C. Fang, Z.-L. Wu, C.-G. Huang, and C.-W. Wu, Review on Residual Stress in Selective Laser Melting Additive Manufacturing of Alloy Parts, *Opt. Laser Technol.*, 2020, **129**, p 106283. https://doi.org/10.1016/j.optlastec.2020.106283
28. S. Gao, Z. Tan, L. Lan, G. Lu, and B. He, Experimental Investigation and Numerical Simulation of Residual Stress and Distortion of Ti6Al4V Components Manufactured Using Selective Laser Melting, *J. Mater. Eng. Perform.*, 2022, **31**(10), p 8113–8123. https://doi.org/10.1007/s11665-022-06815-3
29. T. Larimian, B. AlMangour, D. Grzesiak, G. Walunj, and T. Borkar, Effect of Laser Spot Size, Scanning Strategy, Scanning Speed, and Laser Power on Microstructure and Mechanical Behavior of 316L Stainless Steel Fabricated via Selective Laser Melting, *J. Mater. Eng. Perform.*, 2022, **31**(3), p 2205–2224. https://doi.org/10.1007/s11665-021-06387-8
30. B. AlMangour, D. Grzesiak, and J.-M. Yang, Scanning Strategies for Texture and Anisotropy Tailoring during Selective Laser Melting of TiC/316L Stainless Steel Nanocomposites, *J. Alloys Compd.*, 2017, **728**, p 424–435. https://doi.org/10.1016/j.jallcom.2017.08.022
31. Q. Chao, S. Thomas, N. Birbilis, P. Cizek, P.D. Hodgson, and D. Fabijanic, The Effect of Post-processing Heat Treatment on the Microstructure, Residual Stress and Mechanical Properties of Selective Laser Melted 316L Stainless Steel, *Mater. Sci. Eng. A*, 2021, **821**, p 141611. https://doi.org/10.1016/j.optlastec.2020.106283
32. X. Jiang, W. Xiong, L. Wang, M. Guo, and Z. Ding, Heat Treatment Effects on Microstructure-Residual Stress for Selective Laser Melting AlSi10Mg, *Mater. Sci. Technol.*, 2020, **36**(2), p 168–180. https://doi.org/10.1080/02670836.2019.1685770
33. J. Kluczyński, L. Śnieżek, K. Grzelak, A. Oziębło, K. Perkowski, J. Torzewski, I. Szachogłuchowicz, K. Gocman, M. Wachowski, and B. Kania, Comparison of Different Heat Treatment Processes of Selective Laser Melted 316L Steel Based on Analysis of Mechanical Properties, *Materials*, 2020, **13**(17), p 3805. https://doi.org/10.3390/ma13173805
34. J. Ge, S. Pillay, and H. Ning, Post-process Treatments for Additive-Manufactured Metallic Structures: A Comprehensive Review, *J. Mater. Eng. Perform.*, 2023, **32**(16), p 7073–7122. https://doi.org/10.1007/s11665-023-08051-9
35. M. Waqas, D. He, Y. Liu, S. Riaz, and F. Afzal, Effect of Heat Treatment on Microstructure and Mechanical Properties of Ti6Al4V Alloy Fabricated by Selective Laser Melting, *J. Mater. Eng. Perform.*, 2023, **32**(2), p 680–694. https://doi.org/10.1007/s11665-022-07106-7
36. I. Morozova, C. Kehm, A. Obrosov, Y. Yang, K.U.M. Miah, E. Uludintceva, S. Fritzsche, S. Weiß, and V. Michailov, On the Heat Treatment of Selective-Laser-Melted 316L, *J. Mater. Eng. Perform.*, 2023, **32**(10), p 4295–4305. https://doi.org/10.1007/s11665-022-07404-0
37. S. Liu, C. Liu, and C. Yuan, Effect of Laser Energy Density and Scanning Strategy on Residual Stress in Laser Melting Deposited FGH4096 Superalloy, *J. Mater. Eng. Perform.*, 2024 https://doi.org/10.1007/s11665-024-09152-9
38. I.I. Gorbachev and V.V. Popov, Analysis of the Solubility of Carbides, Nitrides, and Carbonitrides in Steels using Methods of Computer Thermodynamics: III. Solubility of Carbides, Nitrides, and Carbonitrides in the Fe-Ti-C, Fe-Ti-N, and Fe-Ti-C-N Systems, *Phys. Met. Metallogr.*, 2009, **108**(5), p 484–495. https://doi.org/10.1134/S003191X09110088
39. Z. JIS, 2201. *Test Pieces for Tensile Test for Metallic Materials*. (Japanese Standards Association, 1998)
40. D. Wang, C. Song, Y. Yang, and Y. Bai, Investigation of Crystal Growth Mechanism during Selective Laser Melting and Mechanical Property Characterization of 316L Stainless Steel Parts, *Mater. Des.*, 2016, **100**, p 291–299. https://doi.org/10.1016/j.matdes.2016.03.111
41. T. Takaki, Y. Takahashi, and S. Sakane, Multi-Phase-Field Framework for Epitaxial Grain Growth in Selective Laser Melting Additive Manufacturing with Multi-track and Multi-layer, *Mater. Trans.*, 2023, **64**(6), p 1150–1159. https://doi.org/10.2320/matertrans.MT-ME2022014
42. B. Zheng, Y. Zhou, J.E. Smugeresky, and E.J. Lavernia, Processing and Behavior of Fe-Based Metallic Glass Components via Laser-Engineered Net Shaping, *Metall. Mater. Trans. A*, 2009, **40**(5), p 1235–1245. https://doi.org/10.1007/s11661-009-9828-y
43. P.R. Goulart, J.E. Spinelli, N. Cheung, and A. Garcia, The Effects of Cell Spacing and Distribution of Intermetallic Fibers on the Mechanical Properties of Hypoeutectic Al-Fe alloys, *Mater. Chem. Phys.*, 2010, **119**(1), p 272–278. https://doi.org/10.1016/j.matchemphys.2009.08.063
44. O.O. Salman, C. Gammer, A.K. Chaubey, J. Eckert, and S. Scudino, Effect of Heat Treatment on Microstructure and Mechanical Properties of 316L Steel Synthesized by Selective Laser Melting, *Mater. Sci. Eng. A*, 2019, **748**, p 205–212. https://doi.org/10.1016/j.msea.2019.01.110
45. Y. Hong, C. Zhou, Y. Zheng, L. Zhang, and J. Zheng, The Cellular Boundary with High Density of Dislocations Governed the Strengthening Mechanism in Selective Laser Melted 316L Stainless Steel, *Mater. Sci. Eng. A*, 2021, **799**, p 140279. https://doi.org/10.1016/j.msea.2020.140279
46. R. Abbaschian and R.E. Reed-Hill, *Physical Metallurgy Principles*. (Cengage Learning, 2008). https://books.google.com.tr/books?id=wh4v6UWjYdIC
47. H.-Z. Jiang, Z.-Y. Li, T. Feng, P.-Y. Wu, Q.-S. Chen, Y.-L. Feng, L.-F. Chen, J.-Y. Hou, and H.-J. Xu, Effect of Process Parameters on Defects, Melt Pool Shape, Microstructure, and Tensile Behavior of 316L Stainless Steel Produced by Selective Laser Melting, *Acta Metall. Sin. (Engl. Lett.)*, 2021, **34**, p 495–510. https://doi.org/10.1007/s40195-020-01143-8
48. S. Ahmadi Miab, B. Avishan, and S. Yazdani, Wear Resistance of Two Nanostructural Bainitic Steels with Different Amounts of Mn and Ni, *Acta Metall. Sin. (Engl. Lett.)*, 2016, **29**(6), p 587–594. https://doi.org/10.1007/s40195-016-0424-z
49. S. Ghatrehsamani, S. Akbarzadeh, and M. Khonsari, Experimental and Numerical Study of the Running-in Wear Coefficient during Dry Sliding Contact, *Surf. Topogr. Metrol. Prop.*, 2021, **9**(1), p 015009. https://doi.org/10.1088/2051-672X/abbd7a